Journal of Marine Science and Technology

Volume 20 | Issue 6 Article 6

AN OBJECT-ORIENTED ANALYSIS FOR CHARACTERIZING THE RAINFALL-INDUCED SHALLOW LANDSLIDE

Kuan-Tsung Chang
Department of Civil Engineering and Environmental Informatics, Minghsin University of Science and Technology, Hsin-Chu, Taiwan, R.O.C., ktchang1216@gmail.com

Jin-King Liu
LiDAR Technology Co., Chubei City, Hsin-Chu, Taiwan, R.O.C.

Chu-I Wang
Institute of Civil Engineering and Environmental Informatics, Minghsin University of Science and Technology, Hsin-Chu, Taiwan, R.O.C.

Journal of Marine Science and Technology, Vol. 20, No. 6, pp. 647-656 (2012)
DOI: 10.6119/JMST-012-0430-2

AN OBJECT-ORIENTED ANALYSIS FOR CHARACTERIZING THE RAINFALL-INDUCED SHALLOW LANDSLIDE

Kuan-Tsung Chang[1], Jin-King Liu[2], and Chu-I Wang[3]

Key words: landslides, SPOT, LiDAR, segmentation, SVM.

ABSTRACT

Landslides are natural phenomena for the dynamic balance of the earth's surface. Because of frequent occurrences of typhoons and earthquakes in Taiwan, mass movements are common threats to people's lives. In this paper, the interpretation of knowledge is quantified as recognition criteria. Multi-source high-resolution data, for example, a SPOT satellite image, 20 m × 20 m Digital Terrain Model (DTM) reduced from Light Detection And Ranging (LiDAR) data, and aerial orthophotos were used to construct the feature space for landslide analysis. Landslides were recognized by an object-oriented method combining edge-based segmentation and a Supported Vector Machine (SVM) method. The classification results are evaluated in comparison with those by manual interpretation. Two cases from northern and central Taiwan are tested. Both cases show that the object-based SVM method is better than a pixel-based method in classification accuracy. The commission error of the proposed method is also smaller than that of the pixel-based method. Moreover, except for the spectral features, the slope and Object Height Model (OHM) characteristics are also important factors for improving landslide classification accuracy. Further study is required for assessing the mixed pixel effect when the resolution is as large as 20 m and for characterizing the effects of sampling rates or scaling caused by changes in resolution.

I. INTRODUCTION

1. Motivation and Related Work

The World Bank (2005) released a report entitled "Natural Disaster Hotspots: A Global Risk Analysis," stating that approximately 73% of the Taiwan land area and population is exposed to 3 or more risks of natural disasters [13]. Taiwan has a land area of 36,000 m^2, 26.68% of which is covered by planes, whereas 27.31% is hilly and 46.01% is mountainous. By official definition for the purpose of land conservation management, hilly land refers to areas between 100 m and 1,000 m Above Mean Sea Level (AMSL) or areas under 100 m but with a slope greater than 5%. Mountainous land refers to areas with an altitude higher than 1,000 m AMSL [28].

According to statistics of the National Fire Agency (NFA), 270 natural disaster events have occurred in Taiwan from 1958 to 2007. These include typhoons (71.1%), flooding (15%), earthquakes (8.5%), torrential rainfall (2.2%), wind storms (1.5%), mountain flooding (0.7%), and landslides (0.7%) [34]. Taiwan is located in the northwest of the Pacific Ocean, on the major tracks of typhoons. On average, approximately 5 typhoons are likely to affect Taiwan per year. The frequency of natural disasters is on an increasing trend. In total, 89% of the events concern rainfall hazards, with 97% directly or indirectly concerning landslides. Rainfall landslides are a critical issue in managing natural disasters [28, 29]. Moreover, typhoons in Taiwan cause enormous economic losses estimated at approximately US$6 billion per year.

Landslides are a natural phenomenon for the dynamic balance of the earth's surface. The potential or intrinsic factors of landslides include geological and morphological factors. The external or triggering factors include earthquakes, climate, hydrology, and human activities. In Taiwan, the geology is highly fractured and landforms are in high relief. In addition, frequent earthquakes combined with heavy rainfall impose further stress to the earth's surface, with mass movements such as landslides, slumping, and mudflows occurring frequently.

Three types of landslide survey methods exist: ground, aerial, and space-borne [16, 40], or a combination [15]. Ground survey can be highly accurate, but is slow. When hazards occur, accessibility is low. Therefore, it is impossible to make the survey in near real-time or in a large coverage area after a torrential rainfall. The photographic or image interpretation approach can be adopted and implemented manually, auto-

Paper submitted 12/22/11; revised 02/27/12; accepted 04/30/12. Author for correspondence: Kuan-Tsung Chang (e-mail: ktchang1216@gmail.com).
[1] *Department of Civil Engineering and Environmental Informatics, Minghsin University of Science and Technology, Hsin-Chu, Taiwan, R.O.C.*
[2] *LiDAR Technology Co., Chubei City, Hsin-Chu, Taiwan, R.O.C.*
[3] *Institute of Civil Engineering and Environmental Informatics, Minghsin University of Science and Technology, Hsin-Chu, Taiwan, R.O.C.*

matically, or semi-automatically. Manual interpretation requires that a well-trained geologist delineate landslides under a stereoscopic environment, which is time- and labor-intensive [29]. Through the use of criteria for visual interpretation, artificial intelligence of expert systems and automatic procedures can be developed to improve the efficiency and accuracy of landslide mapping [26]. Several investigators have attempted to identify landslides by pixel-based supervised classification methods, for example, Maximum Likelihood (ML) [39] and the Artificial Neural Network method [1, 7, 8, 36]. The advantage for image classification is the objectiveness of these approaches. However, traditional classification methods such as ML are limited by a priori statistical assumptions, for example, a probability distribution and the Hughes Effect, denoting that increasing data bands imposes a need to increase training samples. More than 50% of rainfall-induced landslides in Taiwan are less than 50 m in length. Landslides of this scale are not readily identifiable by their outer shapes using images of a pixel size larger than 10 m. For the resolution limitation and properties for pixel-based classification, landslides can occupy only one or a few pixels without forming an outer shape of a landslide. The pixel-based methods must then be replaced with approaches based on objects or regions [25]. Object-oriented analysis (OOA) is inherently more suitable because it can address the phenomena under study, including landslides, as if they are "objects," and not "pixels" that have spectral, spatial, and contextual characteristics [6, 18, 33, 38]. In addition, this method clearly has the effect of reducing the "salt-and-pepper" appearance typical of the thematic maps generated by conventional pixel-based classification [3, 22]. Because regions are composed of homogeneous pixels, the total number of regions is substantially less than that of pixels in a study area. Thus, efficiency can be improved significantly [17]. However, corresponding experiments showed that if initial segmentation does not correspond with the boundaries of the real-world objects of interest, the classification cannot provide meaningful results [33]. In addition, users must understand the objects under classification for setting proper decision rules of the classifier, including many parameters, weighting factors, and so on.

Different approaches of remotely sensing data exist, including aerial photography, optical satellites, synthetic aperture radar imagery, and topographic data acquisition. They can all be used for landslide inventory [1, 8, 12, 28, 34]. Aerial photography has long been extensively used to characterize landslides and to produce landslide inventory maps, particularly because of their stereo-viewing capability and high spatial resolution [30]. Satellite imagery can also be used to extract information of geological features, geomorphology, land use, hydrology, and so on. However, most landslide detection is based chiefly on spectral features of remotely sensed images other than topographic features. Because the spectral features of buildings and roads are similar to those of landslides, serious misjudgments can occur [36]. Current airborne LiDAR can collect multiple laser returns at pulse repetition rates of up to 500 kHz. The positional accuracy of the resultant laser pulse return is typically at the decimeter level. The obtained standard products of an airborne LiDAR survey thus include all points, ground points, the Digital Surface Model (DSM), and the Digital Elevation Model (DEM). LiDAR DEM has been used for landslide interpretation [14, 22, 37], whereas DSM is not applied as frequently [8]. The integration of multi-source data, including elevation information, has been shown to be extremely useful for landslide inventory [5, 35]. Therefore, the purpose of this study was to use an OOA method with integrated spectral and geomorphometric features for landslide extraction. We also assessed the accuracy of this method. Geomorphometric features were generated from LiDAR's DEM and DSM. The OOA method combined edge-based segmentation and a Support Vector Machine (SVM) classification. The accuracy assessment was made by comparing results of OOA with those from conventional pixel-based methods.

II. METHODOLOGY

The physical appearance of landslides forms the basis for recognizing the boundary and type of a landslide. However, displaced material of a rainfall-induced landslide is usually washed away from steep slopes. What remain are only the fresh scars of the ruptured surface. The fresh landslide scars at var-ious slope gradients and locations normally include landslide types such as rock falls, debris slides, channel bank failures, and debris flows. In this study, the landslides concerned covered all these types except debris flows. The exception was because debris flows are triggered by a different mechanism, with more contributions from flowing water instead of gravity. In other words, debris flows can be treated as a transformation of other shallow-seated landslides when a high concentration of rainfall and liquefaction of displaced materials occur [28]. The principle of the proposed object-oriented workflow combining an edge-based segmentation and SVM classification for automatic landslide interpretation is as follows. The segmentation procedure is used first on the partition of digital feature data into multiple regions (set of pixels) based on given criteria. After segmentation, each region is assigned a unique label. However, the labeled regions should be reclassified into desired classes, as defined. Therefore, a supervised classification method is used next to derive the final result of landslide interpretation in this study.

1. Edge-Based Segmentation Method

A basic task of segmentation algorithms is the merging of image elements based on homogeneity parameters or on the differentiation to neighboring regions (i.e., heterogeneity). Thus, segmentation methods follow 2 strongly correlated principles of neighborhood and similarity of pixel values. Generally, edge-based and region-based methods can be applied to partition a scene into regions [4].

Region-based approaches start in image space where the

available elements, either pixels or already existing regions, are tested for similarity against other elements. Region growing (i.e., bottom-up, starting with a seed pixel) and region splitting (i.e., top-down, starting with the entire scene) procedures are distinguished to define initial segmentation. One disadvantage of the splitting method is that it tends to be over-segmented because splitting always produces a fixed number of sub-regions (normally 4), although 2 or 3 of them might actually be homogeneous with respect to each other. Consequently, one can apply an integration of the various methods. Thus, it leads to the split-and-merge algorithm, such that, after a split process, if neighboring regions are similar, they should be remerged. To strengthen the automation of segmentation, clustering is adopted for region-based segmentation. An Iterative Self-Organizing CLUSTering (ISOCLUST) method is an unsupervised classifier based on a concept similar to the well-known ISODATA routine of Ball and Hall and cluster routines such as the H-means and K-means procedures [21]. The authors compared 2 region-based segmentation methods named thresholding and the ISOCLUST method with the ground truth extracted on the basis of orthophotos and DSM-shaded relief images of the experimental area. The experimental results showed that the thresholding met more closely with the ground truth, whereas the ISOCLUST method was able to demonstrate details of the landslide features though omission error prevailed [9]. The multi-resolution segmentation used in the eCognition Professional developed by Definiens Image is a process controlled by scale, shape, color, compactness, and smoothness parameters [33]. It is a bottom-up pairwise region-merging algorithm, where the appropriate values of all parameters used in the method should be determined by trial-and-error tests [22].

Edge-based approaches describe regions by their outlines. These are generated through edge detection filtering, for example, a Sobel or Canny operator, followed by an edge-linking algorithm. Optionally, the transition from the outlines to the interior region can be achieved by contour-filling methods such as the morphological watershed algorithm. The main disadvantage of edge-based approaches is that the edge and the contour image are affected strongly by noise, which may lead to unacceptable over-segmentation. Two ways of solving the over-segmentation problem are to merge adjacent similar regions iteratively or to build a watershed hierarchy using different scale spaces [23].

Therefore, an edge-based segmentation algorithm as used in this study was fast and required only one input parameter (**Scale Level**) . By suppressing weak edges to different levels, the algorithm yielded multiscale segmentation results from finer to coarser segmentation. First, the used segmentation algorithm was used to calculate a gradient map and its corresponding density function (called cumulative relative histogram) for the whole image. A sub-image window was then selected to compute a modified gradient map using the original gradient map, density function, and **Scale Level** . The watershed transform was applied on the modified gradient map for the sub-image to determine an acceptable scale parameter according to the segmented result for sub-images iteratively. Finally, the watershed transform was reapplied to segment the modified gradient map for the whole image [20, 23]. Prior to segmenting the modified gradient map, a sub-image can be segmented at the selected scale level to determine if the scale level provides the desired segmentation. The used edge-based segmentation method can overcome the mentioned disadvantage for other edge-based segmentation methods, for example, broken edges or over-segmentation. Moreover, its computation performance (computational complexity is O(n)) is among the fastest segmentation algorithms. The ability to perform a result preview and sub-image segmentation can reduce a tedious and time-consuming trial-and-error process where a reasonable scale parameter is found [23].

2. Support Vector Machine Method

The supervised classification can be considered one of the modeling probability distributions [3]. SVM is a relatively new supervised classifier and is based on strong foundations from statistical learning theory. Since its inception in the early 1990s, it has found applications in a wide range of pattern recognition problems, image classification, financial time series prediction, face detection, biomedical signal analysis, medical diagnostics, and data mining [10, 19]. It separates 2 classes with a decision surface that maximizes the margin between the classes. The surface is often called the optimal hyperplane, and the data points closest to the hyperplane are called support vectors. The support vectors are the critical elements of the training set [11].

Under the basic assumption of the SVM approach, the training sample is expressed as follows:

$$w^T x_i + b = 0 \tag{1}$$

The weighing vectors w and b are deemed satisfactory once they are converged.

$$y_i(w^T x_i + b) \geq 1 - \varepsilon \tag{2}$$

The ε value is a loose variable existing in a linear, undividable condition. It describes the degree of module deviation under the ideal linear circumstances. The goal of the SVM is to identify a decision support phase where the average error of the training samples is minimized. The optimization equation is therefore derived as follows:

$$\varphi(w, \varepsilon) = \frac{1}{2} w^T w + C \sum_{i=1}^{N} \varepsilon^i \tag{3}$$

where C is a positive parameter assigned by the end user. It serves as a penalty for the correctness of the SVM. The C value is used to leverage the probable misinterpretation percentage and the complexity of the algorithm. A converged

optimization equation can be derived adopting the Lagrange multiplication method:

$$Q(\alpha)=\sum_{i=1}^{N}\alpha_i-\frac{1}{2}\sum_{i=1}^{N}\sum_{j=1}^{N}\alpha_i\alpha_j y_i y_j K(x_i,x_j) \quad (4)$$

where $\{\alpha_i\}_{i=1}^{N}$ is the Lagrange multiplier, and Eq. (4) fulfills the following criteria:

$$\sum_{i=1}^{N}\alpha_i y_i=0,\ 0\le\alpha_i\le C,\ \ i=1,2,3,\cdots N \quad (5)$$

$K(x_i,x_j)$ is a kernel function. After kernelization, the SVM can be applied to situations in which 2 classes are not linearly separable [3]. Four types of kernel functions are included in the Mercer theorem:

1. Linear:

$$K(x_i,x_j)=x_i^T x_j \quad (6)$$

2. Polynomial

$$K(x_i,x_j)=(\gamma x_i^T x_j+r)^d,\ \gamma>0 \quad (7)$$

3. Radial Basis Function (RBF):

$$K(x_i,x_j)=\exp(-\gamma\left\|x_i-x_j\right\|^2),\ \gamma>0 \quad (8)$$

4. Sigmoidal:

$$K(x_i,x_j)=\tanh(\gamma x_i^T x_j+r),\ \gamma>0 \quad (9)$$

Here, γ, r, and d are kernel parameters [2, 24].

SVM can be adapted to become a nonlinear classifier through use of nonlinear kernels. Although SVM is a binary classifier in its simplest form, it can function as a multiclass classifier by combining several binary SVM classifiers (creating a binary classifier for each possible pair of classes). For comparison, the SVM function built in an ENVI software developed by ITT Co. was used after the segmentation. The most popular kernel in the SVMs is the RBF kernel, which functions well in most cases and was, therefore, chosen in this study. The parameter essentially determines the training/testing trade-off when it sets a large value that leads to overfit [3].

To recognize landslides, the authors compared the pixel-based SVM by using the Back-Propagation Neural Network (BPNN) and an ML method. Results showed that the recognition accuracy for the BPNN and pixel-based SVM method are better than the ones for the ML method [6]. A superiority of the SVMs for remote sensing image classification over neural networks is the unambiguity of the solution. Because one maximizes a quadratic function, the extreme is global and is always found. No possibility exists of becoming trapped in a local maximum [3].

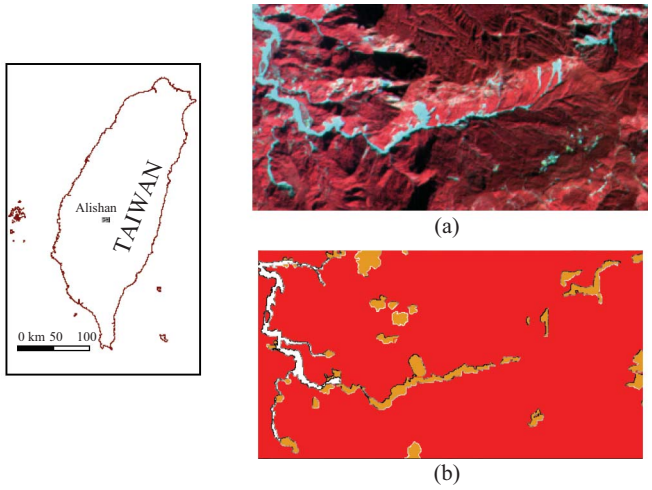

Fig. 1. (a) Satellite image of the Alishan study area and (b) its ground truth.

III. CASE STUDY

1. Two Test Areas and Their Ground Truths

Two test areas were selected for this study. The first test area is located at the Alishan upstream basin near central Taiwan. The Alishan study area has an area of approximately 36 km^2. The geological formations are composed of alternations of highly fractured sandstone and shale. In the study area, the accumulated rainfall reached 811 mm in 24 h and 1,200 mm in 48 h since 2006 June 9. This heavy rainfall event, called the six-nine torrential rainfall, induced enormous amounts of debris flows and slides. LiDAR data were acquired by a Leica ALS50 airborne LiDAR system. Both LiDAR data and aerial photographs were taken in 3 d on June 18, June 19, and June 22 of 2006. The point density of LiDAR point clouds was approximately 4 points/m^2. Moreover, SPOT-5 multispectral satellite images containing green (G), red (R), and near-infrared bands (NIR) (Fig. 1(a)) were used. No record of heavy rainfall events one year prior to this event exist. The landslides observed with these data sets could be attributed solely to this torrential rainfall event.

The second experiment was conducted using a LiDAR data set in Yilan County of eastern Taiwan, acquired after Typhoon Kalmaegi, which affected Taiwan area from July 16 to July 18, 2008. Data acquisition using a Leica ALS50 airborne LiDAR system was conducted on 2008 November 4. The point density of all points was 1.454/m^2 and that of ground points was 0.454/m^2. The orthophoto used in this study is shown in Fig. 2(a).

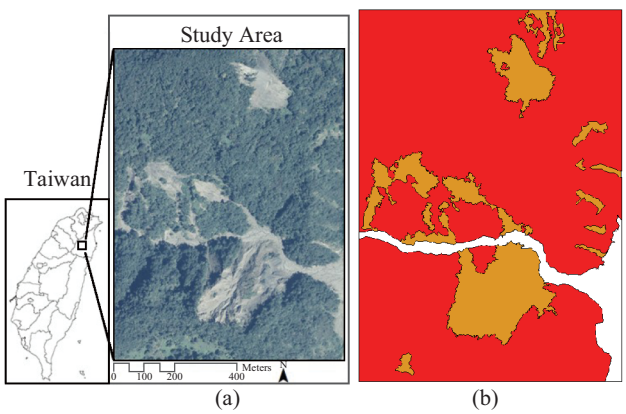

Fig. 2. (a) The aerial photo of the Yilan study area and (b) its ground truth.

The perception of landslides from a bird's eye view of aerial photographs largely depends on the scale or spatial resolution of the photographs. Six criteria can be used for the visual recognition of landslides on aerial photographs, including tone, location, shape, direction, slope, and shadow effects. According to these expert criteria, orthophotos and corresponding river and road maps were imported into the ArcGIS 9.2 software to aid in the visual digitization of the 3 classes. The results of manual air-photo interpretation as shown in Figs. 1(b) and 2(b) could be used as the ground truth. The pixels in brown, red, and white indicate landslide area, vegetation, and river bed, respectively.

2. Experimental Workflow and Interpretation Keys

The detailed experimental workflow is shown in Fig. 3. First, an orthophoto or a SPOT multispectral image, LiDAR's DEM and DSM, and corresponding vector data containing river and road maps for the study areas were collected. Manual interpretation was then performed to obtain the ground truth. According to the land-use status of the study areas and the purpose of this study, 3 classes were present for the ground truth needing interpretation, including landslide, river bed, and vegetation. Next, the feature layers required for automatic processing of segmentation were generated from the raw data sets, including spectral and geomorphometric features. If the segmentation and merging results were satisfactory for the experiments, then representative training regions for each land class would be selected. After selection of the training regions, training could be performed for the used SVM classification method. Finally, accuracy assessments of each experiment could be performed based on the classification results and the ground truth. In the accuracy assessment, both the omission error (type I error) and commission error (type II error) should be also considered [27].

Key rules for the automatic landslide interpretation consisted of spectral and geomorphometric features summarized from the literature, case studies, and expert experience. Because newly formed landslides are mostly bare ground, their

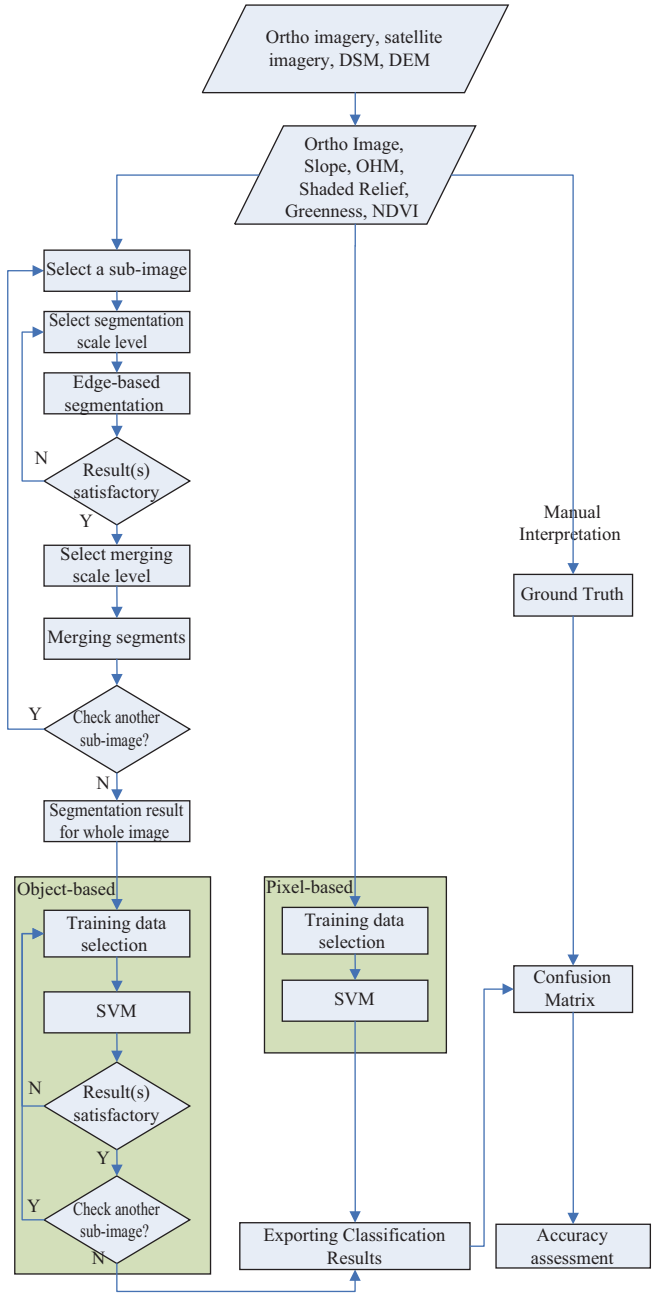

Fig. 3. The experimental workflow in the study.

spectral reflectance curve becomes changed than before. Vegetation indices can be calculated by multispectral satellite images to explore the spectral characteristics of landslides. Among more than 20 types of vegetation indices, a standardized vegetation index called the Normalized Vegetation Index (NDVI) is the most commonly used indicator for surface biomass cover. The NDVI calculation formula is as follows:

$$NDVI = \frac{NIR - R}{NIR + R} \tag{10}$$

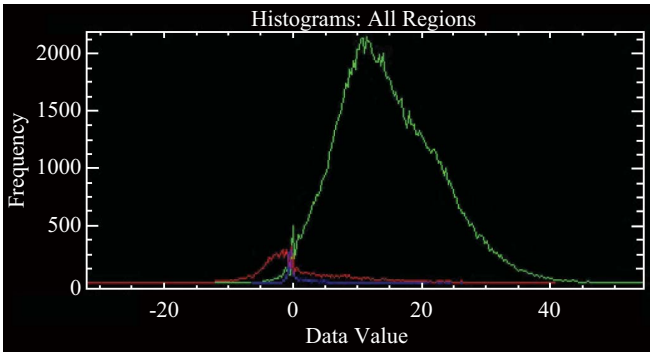

Fig. 4. The NDVI*slope histogram for the ground truth data.

where NIR and R indicate the digital number on the near-infrared band and the red band, respectively. In the second case, because the adopted orthoimage did not cover the near-infrared band, the Green-Red Vegetation Index was used. This index is also called Greenness [22]. Moreover, some geomorphometric features including slope and normalized Digital Surface Model (nDSM, also called OHM) were used in the experiments. If only the spectral characteristics are used for the landslide interpretation, it is difficult to recognize landslides and other land cover classes with similar spectral features (such as bare soil and river). The local slope was calculated using the third-order finite difference weighted by the reciprocality of the squared distance algorithm. The mathematical formula for the slope computation can be found in ref. [39]. OHM obtained by subtraction of DSM and DEM is a normalized height of objects above the bare ground surface. Because the terrain effects have been removed, OHM exhibits a good appearance of landslides [6].

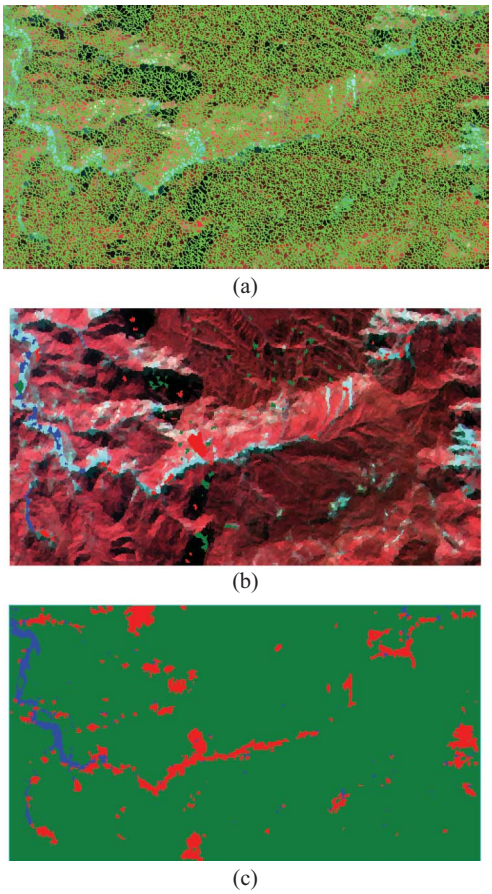

Fig. 5. The best object-based classification result for the Alishan case. (a) Segmentation result, (b) The selected training regions for the object-based SVM method, and (c) Object-based SVM classification result.

IV. EXPERIMENTAL RESULTS AND ANALYSIS

1. The Alishan Upstream Case

SPOT images and airborne LiDAR data were used in this study. Applied feature space includes spectral features such as G, R, IR, and NDVI, and spatial features such as slope and OHM. After a few preliminary experiments, 4 features were selected, including G, R, IR, and NDVI*slope. The "*" in the NDVI*slope feature represents a multiplier of NDVI and slope value. It is a composite feature that possesses a unique capability of enhancement for effective separation of the feature value distribution of a landslide and other land cover classes (e.g., river). A statistical NDVI*slope histogram, as shown in Fig. 4, generated from the ground truth shows that the NDVI*slope value for landslides ranging from a minimum value to -2, and one for a river ranging from -5 to -0.01. Because the resolution of SPOT is 20 m and that of LiDAR is 1 m, the relatively low resolution of SPOT images requires a parameter for segmentation with a low scale level to obtain more detailed regions (or objects). If the scale level is high, more mixed objects are formed and classification accuracy is lower. To assure pure objects that include only one land class, the training objects were not merged for similar classes. Therefore, the only parameter for the segmentation scale level was set to 0, and subsequently, the scale level for merging was set to 0 as well. The object-based classification result for the Alishan case is shown in Fig. 5. A comparison was also made using pixel-based SVM. The parameters used were based on our former study [8]. The pixel-based classification result for this case is shown in Fig. 6.

The analytical results after the Confusion Matrix are shown in Table 1. The accuracy is expressed in percentages. The results show that the producer accuracy (PA) of the object-based and pixel-based SVM methods are 82% and 41%, respectively. User accuracy (UA) of the two SVM methods are 84% and 43%, respectively. The authors used the same training data on the object-based SVM and pixel-based SVM method to evaluate the landslide interpretation. Experimental results indicate that PA and UA accuracy for the pixel-based SVM are only 41% and 43% accurate, respectively. Obvious differences in accuracy exist between the results of OOA and

Table 1. Accuracy comparison between object-based and pixel-based methods for the Alishan case.

Object-based	PA%	UA%	Pixel-based	PA%	UA%
Landslide	81.94	84.44	Landslide	41.34	43.11
River bed	72.29	78.46	River bed	42.02	48.88
Vegetation	99.00	98.65	Vegetation	96.92	96.39
Kappa Coefficient = 0.8246			Kappa Coefficient = 0.4776		
Overall Accuracy = 97.5%			Overall Accuracy = 89.6%		

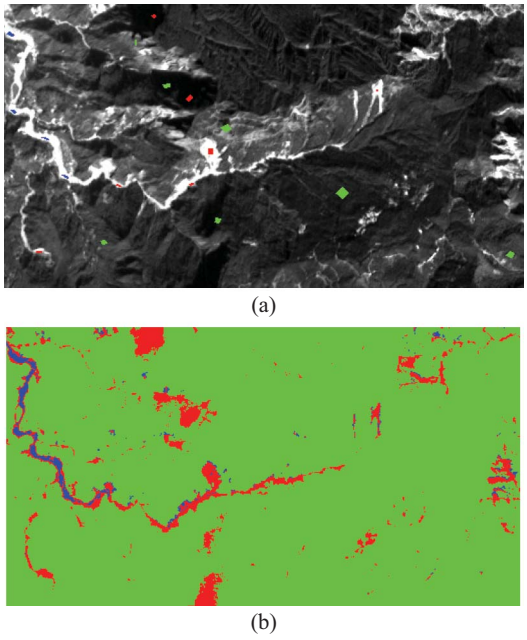

(a) (b)

Fig. 6. The best pixel-based classification result for the Alishan case. (a) The selected training samples for the pixel-based SVM method and (b) Pixel-based SVM classification result.

Pixel-based methods. Evidently, an object-oriented classification approach combining both the edge-based segmentation and supervised SVM classification methods can achieve greater results in landslide assessment than the pixel-based methods.

2. The Yilan Case

In this case, orthophotos had a resolution of 25 cm with that of airborne LiDAR 1 m. The applied feature space included spectral features of G, R, and Greenness, and spatial features of slope and OHM. Results by using spectral features alone for landslide extraction were not good because of spectral similarities between the river bed and landslides. Geomorphological features of rainfall-induced landslides, for example, OHM, have been shown to be useful in the automatic recognition of landslides. Three features of Greenness, OHM, and slope were selected for this experiment after a few trial tests. In addition, because of the high resolution of the data sets, the scale level for segmentation could be set with a high value other than 0. Regions with similar attributes could also be merged. The adverse effect of mixed pixels was low under the high scale level of segmentation and merging. The optimal scale level for segmentation was 2.5 and that for merging was 85 after trials. A pixel-based SVM method was also adopted for conducting a similar procedure of comparison as with the Alishan case. After trials, we obtained the best classification results for the object-based SVM and pixel-based SVM methods, which are shown in Figs. 7 and 8, respectively.

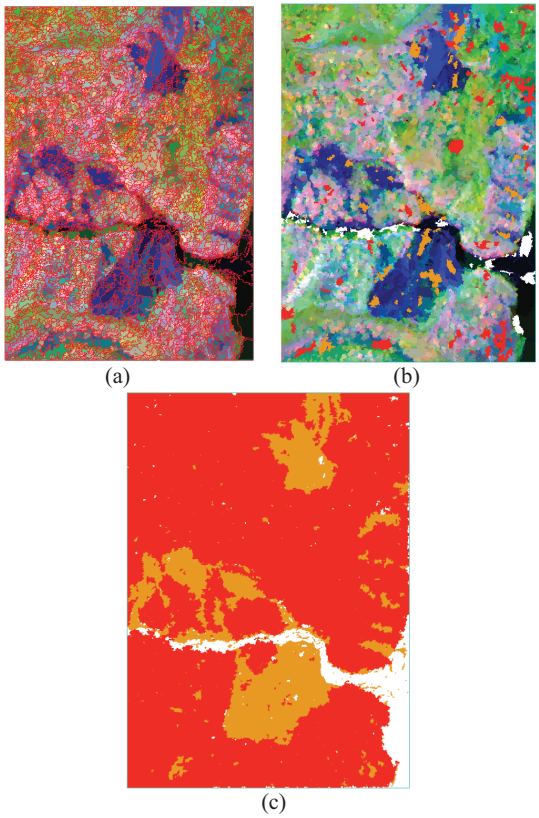

(a) (b) (c)

Fig. 7. The best object-based classification result for the Alishan case. (a) Segmentation result for the Yilan case, (b) The selected training regions for the object-based SVM method, and (c) Object-based SVM classification result.

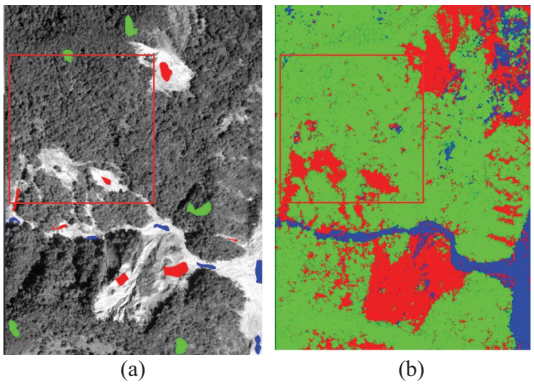

(a) (b)

Fig. 8. The best pixel-based classification result for Yilan case. (a) The selected training samples for the pixel-based SVM method and (b) Pixel-based SVM classification result.

Table 2. Accuracy comparison between object-based and pixel-based methods for the Yilan case.

Object-based	PA%	UA%	Pixel-based	PA%	UA%
Landslide	85.68	80.41	Landslide	72.01	76.20
River bed	83.21	87.81	River bed	70.88	76.20
Vegetation	95.72	96.59	Vegetation	94.55	93.53
Kappa Coefficient = 0.8170			Kappa Coefficient = 0.7043		
Overall Accuracy = 93.4%			Overall Accuracy = 89.6%		

Table 2 shows the confusion matrix or accuracy table of the results. The accuracy is expressed in percentages. The results show that the producer accuracy of the object-based and pixel-based SVM method was 86% and 81%, respectively. The user accuracy of the 2 SVM methods was 80% and 52%, re-spectively. The assessment using the same training data was also applied on this test case; however, despite the UA accuracy for the pixel-based SVM method increasing to 76%, the PA accuracy decreased to 72%. The differences in UA accuracy are significantly . We obtained a similar trend for the classes of riverbeds and vegetation. Evidently, an object-oriented classification approach combining both the edgebased segmentation and supervised SVM classification methods could achieve greater results in landslide assessments than the pixel-based methods.

For the interpretation keys, in addition to spectral features, spatial features such as slope or OHM were also important factors for landslide classification, both for object-based and pixel-based methods. Such features must be defined in relation to local conditions and the specific events triggering the land-slides [28, 31, 32]. However, spatial features contributed little to the classification accuracy in the Alishan case. The reason may be due to the incompatibility between the spectral images and DTM used. Finally, used data, feature indices, and corresponding setting for parameters related to the OOA method can be summarized as shown in Table 3.

Table 3. The parameters setting in the OOA.

	Test area #1-Alishan case	Test area #2-Yilan case
Used data	SPOT-5 satellite image LiDAR DEM, DSM Topographic maps	Aerial orthophoto LiDAR DEM, DSM Topographic maps
Spatial resolution	20 meter	1 meter
Used features	G, R, IR, NDVI*Slope	Greenness, Slope, OHM
Segment scale level	0	2.5
Merge scale level	0	85
Classifier	Object-based SVM Pixel-based SVM	Object-based SVM Pixel-based SVM
SVM Kernel	RBF kernel function	RBF kernel function
SVM parameters	Gamma (γ) in RBF Kernel (default value is 1.000) Penalty Parameter C (default value is 100.00)	

V. CONCLUSIONS AND SUGGESTIONS

1. Conclusions

We adopted an OOA method in this study to extract landslide features. We assessed its performance for accuracy in 2 cases integrating multi-resolution digital data, for example, aerial or satellite imagery, terrain data derived from an airborne LiDAR sensor, and its derivative indicators including slope and OHM in the landslide interpretation. We also compared these data with a conventional pixel-based SVM method. We applied edge-based segmentation first, and then merged similar attributes. Subsequently, we selected patches of training samples for an SVM classification.

Our conclusions from the experimental results are as follows:

1. In general, the resolution of the feature layers in feature space is an important characteristic for both pixel-based and object-based analyses. Better resolution usually generates improved accuracy. The accuracy of the vegetation class was as high as 82% for PA and 95% for UA. These results show that the spectral information of vegetation suffices for the recognition of the biomass-rich class.
2. Spectral features cannot be applied effectively for landslide recognition without additional input from spatial information. Geomorphological features of rainfall-induced landslides, such as slope and OHM, are useful in the automatic recognition of landslides. However, in the Alishan case, spatial information did not contribute substantially in improving accuracy because the resolution for SPOT images (20 m) does not conform with that of LiDAR DEM (1 m).
3. Parameters for segmentation and object merging depend on the resolution of images. In this study, when ground resolution was as small as 1 m, the optimal scale level for segmentation was 2.5, and that for merging was 85. When the ground resolution was 20 m, and the optimal scale level for both segmentation and merging was set to 0, to avoid the adverse effect of mixed pixels.
4. One of the advantages of the method raised in this study is that it is not dependent on sound rules for interested classes. Initially, only limited training samples are required and selected manually. Subsequently, rules can be established automatically by using the attributes of the considered objects. The SVM algorithm automatically converges the attributes for selected training samples.
5. Rules for classification using eCognition must be prepared adequately, including all settings for segmentation and merging. Results generated in each step can be visu-alized and inspected for further modification. Human expert knowledge is thus implemented in the analytical processes. This is one of the most important advantages of this method.

2. Suggestions

1. In the future, significant geomorphological features such as roughness and diversity should be considered to evaluate and improve object-oriented classification accuracy.
2. Future research should confirm the causes of erroneous judgments in the procedures for the landslide inventory. The method applied in this study has the advantage of a knowledge base of rules that can be applied in similar cases. Rules for interested classes can be further ana-lyzed to verify their contribution to the final accuracy.

REFERENCES

1. Barlow, J., Martin Y., and Franklin, S. E., "Detecting translational landslide scars using segmentation of Landsat ETM+ and DEM data in the northern Cascade Mountains, British Columbia," *Canadian Journal of Remote Sensing*, Vol. 29, No. 4, pp. 510-517 (2003).
2. Burges, J., "A tutorial on support vector machines for pattern recongnition," *Data Mining and Knowledge Discovery*, Vol. 2, pp. 121-167 (1998).
3. Canty, M. J., *Image Analysis, Classification, and Change Detection in Remote Sensing : With Algorithms for ENVI/IDL*, CRC Press, Taylor & Francis Group (2010).
4. Carleer, A., Debeir, O., and Wolff, E., "Comparison of very high spatial resolution satellite image segmenations," *Proceedings of SPIE Image and Signal Processing for Remote Sensing IX*, Vol. 5238, pp. 532-542 (2004).
5. Chang, K. T., Hwang, J. T., Liu, J. K., Wang, E. H., and Wang, C. I., "Apply two hybrid methods on the Rainfall-induced landslides interpretation," *Geoinformatic 2011*, Shanghai, China (2011).
6. Chang, K. T., Kao, Q. X., Wang, Z. Y., and Liu, J. K., "Automatic rainfall-induced landslide interpretation and features analysis, special issue for disaster prevention," *Journal of Photogrammetry and Remote Sensing*, Vol. 15, No. 1, pp. 79-95 (2010). (in Chinese)
7. Chang, K. T. and Liu, J. K., "Landslide features interpreted by neural network method," *The International Archives of the Photogrammetry, Remote Sensing and Spatial Information Sciences*, Istanbul, Turkey, Vol. XX, Part B7, pp. 574-579 (2004).
8. Chang, K. T., Liu, J. K., Chang, Y. M., and Kao, C. S., "An accuracy comparison for the landslide inventory with the BPNN and SVM methods," *Gi4DM 2010*, Turino, Italy (2010).
9. Chang, K. T., Wang, Z. Y., Kao, Q. X., and Liu, J. K., "A comparison of two OOA segmentation methods for the detection of rainfall-induced landslides using airborne LiDAR nDSM data," *The 2010 International congress on Computer applications and Computational Science (CACS2010)*, IRAST Press, Singapore (2010).
10. Chapelle, O., Haffner, P., and Vapnik, V., "Support vector machines for histogram-based image lassification," *IEEE Transactions on Neural Networks*, Vol. 10, No. 5, pp. 1055-1064 (1999).
11. Chen, C. C., *Rice Paddy Identification using the Support Vector Machine and Plausible Neural Network*, MSc Thesis, Department of Civil Engineering, NCTU, HsinChu, Taiwan (2006). (in Chinese)
12. Delacourt, C., Allemand, P., Squarzoni, C., Picard, F., Raucoules, D., and Carnec, C., "Potential and limitation of ERS-Differential SAR interferometry for landslide studies in the French Alps and Pyrenees," *Proceedings of FRINGE 2003 Workshop*, Frascati, Italy (2003).
13. Dilley, M., Chen, R. S., Deichmann, U., Lerner-Lam, A. L., Arnold, M., Agwe, J., Buys, P., Kjekstad, O., Lyon, B., and Yteman, G., *Natural Disaster Hotspots: A Global Risk Analysis*, Disaster Risk Management Series No.5, The World Bank, Washington, D.C. (2005).
14. Eeckhaut, V. D., Poesen, M. J., Verstraeten, G., Vanacker, V., Nyssen, J. Moeyersons, Van, J., and Vandekerckhove, L. P. H., "Use of LiDAR-derived images for mapping old landslides under forest," *Earth Surface Processes and Landforms*, Vol. 32, No. 5, pp. 754-769 (2007).
15. Galli, M., Ardizzone, F., Cardinali, M., Guzzetti, F., and Reichenbach, P., "Comparing landslide inventory maps," *Geomorphology*, Vol. 94, pp. 268-289 (2008).
16. Guzzetti, F., Cardinali, M., Reichenbach, P., and Carrara, A., "Comparing landslide maps: a case study in the upper Tiber River Basin, central Italy," *Environmental Management* , Vol. 25, No. 3, pp. 247-363 (2000).
17. Hong, K. C., *Landslide Detection Using Various Features from Multispectral Imagery*, Master Thesis, Department of Geomatics, National Cheng Kung University, Tainan, Taiwan (2009). (in Chinese)
18. Huang, W. K., Lin, M. L., Chen, L. C., Lin, Y. H., and Hsiao, C. Y., "Applying object-oriented analysis to segmentation and classification of landslide and artificial facilities with remote sensing images," *Journal of photogrammetry and remote sensing*," Vol. 15, No. 1, pp. 29-49 (2010). (in Chinese)
19. Hwang, J. and Chiang, H., "The study of high resolution satellite image classification based on Support Vector Machine," *Geoinformatic 2010*, Beijing, China (2010).
20. ITT, *ENVI EX User's* Guide (2010).
21. Jain, A. K. and Dubes, R. C., *Algorithms for Clustering Data*, Prentice Hall, Inc (1988)
22. Jhan, J. P. and Rau J. Y. "A four-stage object-based segmentation and classification scheme for landslide detection," *Proceedings of Asian Conference on Remote Sensing 2011*, Taipei, Taiwan (2011).
23. Jin, X., "Segmentation-based image processing system," US Patent 20090123070, filed Nov. 14, 2007, and issued May 14 (2009).
24. Kao, Q., *Automatic Interpretation and Feature Analysis for the Rain-Fall Induced Landslide*, Master Thesis, Minghsin University of Science and Technology, HsinChu, Taiwan (2010). (in Chinese)
25. Kerle, N. and Martha, T. R., "The potential of object-based and cognitive methods for rapid detection and charcterisation of landslides," *Gi4DM 2010*, Turino, Italy (2010).
26. Kojima, H., Chung, C. F., and Westen, C. V., "Strategy on the landslide type analysis based on the expert knowledge and the quantitive prediction model," *International Archives of Photogrammetry and Remote Sensing*, Vol. XXXIII, Part B7, pp. 701-708 (2000).
27. Lillesand, T. M., Kiefer, R. W., and Chipman, J. W., *Romote Sensing and Image Interpretation*, Fifth Edition, John Wiley & Sons, Inc. (2004).
28. Liu, J. K., Chang, K. T., Rau, J. Y., Hsu, W. C., Liao, Z. Y., Lau, C. C., and Shih, T. Y., *The Geomorphometry of Rainfall-Induced Landslides in Taiwan Obtained by Airborne Lidar and Digital Photography*, Geoscience and Remote Sensing, In-Tech, Inc. (2009).
29. Liu, J. K., Wong, S. J., Huang, J. H., and Huang, M. J., "Images analysis for landslides induced by torrential rainfall," *Proceedings of Symposium on Civil Engineering Technology and Management for 21 Century*, Hsinchu, P.C-21~C-31 (2001).
30. Mantovani, F., Soeters, R., and Van, C. J., "Remote sensing techniques for landslide studies and hazard zonation in Europe," *Geomorphology*, Vol. 15, pp. 213-225 (1996).
31. McKean, J. E., Acker, S. A., Fitt, B. J., Renslow, M., Emerson, L., and Hendrix, C. J., "Objective landslide detectoin and surface morphology mapping using high-resolution airborne laser altimetry," *Geomorphology*, Vol. 57, pp. 331-351 (2004).
32. McKean, N. F., Streutker, D. R., Chadwick, K., Glenn, D. J., Thackray, G. D., and Dorsch, S. J., "Analysis of LiDar-derived topographic information for characterizing and differentiating landslide morphology and activity," *Geomorphology*, Vol. 73, pp. 131-148, DOI: 10.1016/j.geomorph.2005.07.006 (2005).
33. Moine, M., Puissant, A., and Malet, J. P., "Detection of landslides from aerial and satellite images with a semi-automatic method. Application to the Barcelonnette basin (Alpes-de-Haute-Provence, France)," *Landslide Process: from Geomorphological Mapping to Dynamic Modelling*, pp. 63-68 (2009).
34. NFA, "Historical records of natural disasters of Taiwan from 1958 to 2007," National Fire Agency, Ministry of the Interior, Access date: 31 December 2008, http://www.nfa.gov.tw/Show.aspx?MID=97&UID=827&PID=97
35. Nichol, J. and Wong, M. S., "Satellite remote sensing for detailed land-

slide inventories using change detection and image fusion," *International Journal of Remote Sensing*, Vol. 26, No. 9, pp. 1913-1926 (2005).
36. Parise, M., "Landslide mapping techniques and their use in the assessment of the landslide hazard," *Physics and Chemistry of the Earth*, Vol. 26, No. 9, pp. 697-703, DOI: 10.1016/S1464-1917(01)00069-1 (2001).
37. Schulz, W. H., "Landslide susceptibility revealed by LiDAR imagery and historical records," *Seattle, Washington, Engineering Geology*, Vol. 89, Nos. 1-2, pp. 67-87, DOI: 10.1016/j.enggeo.2006.09.019 (2007)
38. Van, S. and Seijmonsbergen, A. C., "Expert-driven semi-automated geomorphological mapping for a mountainous area using a laser DTM," *Geomorphology* Vol. 78, pp. 309-320 (2006).
39. Yang, M. S., *Integrating LiDAR Derived Data and SPOT Multispectral Imagery for Landslides Classification*, MSc Thesis, Department of Geography, NKNU, Kaohsiung, Taiwan (2007). (in Chinese)
40. Zanutta, A., Baldi, P., Bitelli, G., Cardinali, M., and Carrara, A., "Qualitative and quantitative photogrammetric techniques for multi-temporal landslide analysis," *Annals of Geophysics*, Vol. 49, Nos. 4/5, pp. 1067-1080 (2006).